Journal of Micromechanics and Microengineering

TECHNICAL NOTE • **OPEN ACCESS**

Transillumination lab-on-a-chip cytometer with silicon/glass membrane for image-based porcine oocyte deformation characterisation

To cite this article: Aleksandra Pokrzywnicka *et al* 2024 *J. Micromech. Microeng.* **34** 017001

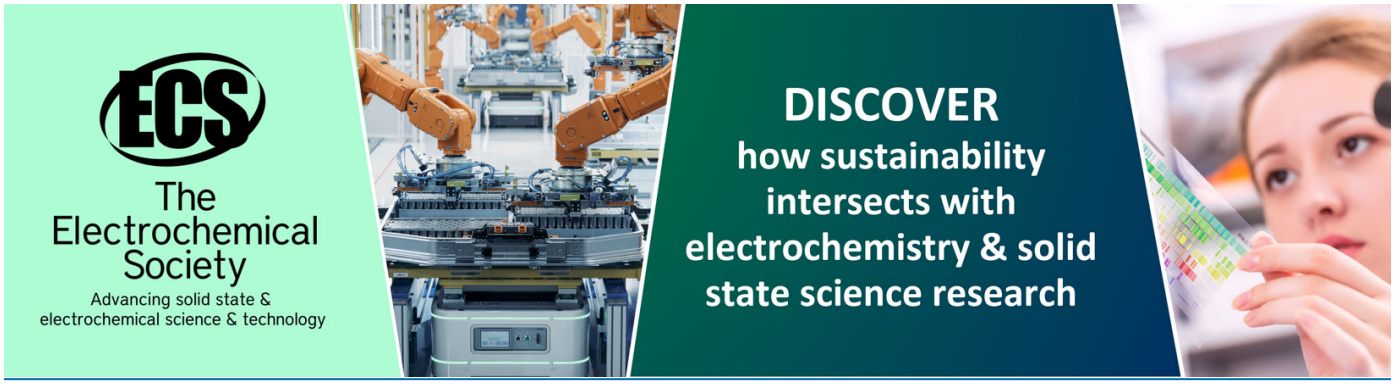

OPEN ACCESS
IOP Publishing
Journal of Micromechanics and Microengineering
J. Micromech. Microeng. **34** (2024) 017001 (7pp)
https://doi.org/10.1088/1361-6439/ad0d81

Technical Note

Transillumination lab-on-a-chip cytometer with silicon/glass membrane for image-based porcine oocyte deformation characterisation

Aleksandra Pokrzywnicka, Danylo Lizanets and Rafał Walczak*

Wroclaw University of Science and Technology, Faculty of Electronics, Photonics and Microsystems, Wroclaw, Poland

E-mail: rafal.walczak@pwr.edu.pl

Received 22 August 2023, revised 24 October 2023
Accepted for publication 16 November 2023
Published 28 November 2023

Abstract

Transillumination microscopes, often with a simple lens-free optical configuration, combined with lab-on-a-chip devices are useful tools for the characterisation of various biological samples. A key issue with these devices is light transparency across a lab-on-a-chip structure. In this work we achieved this by embedding a glass window in a silicon membrane. Despite light transmission, the membrane could be pressure actuated. A second key issue is software analysis of the images due to the holographic nature of the captured images. In this paper, the technology of the silicon/glass membrane and results of porcine oocyte imaging during deformation are presented and compared with our previous micro-electro-mechanical system cytometer working with a reflective microscope. Thus, a unique device that deforms cells and allows deformation measurements with transillumination was developed.

Keywords: MEMS cytometer, transillumination imagining, glass

1. Introduction

Fluidic-based microsystems have the potential to create integrated, miniaturised and stand-alone laboratories, so-called lab-on-a-chip platforms on which different instrumentation and functionalities of biological or chemical laboratories may be applied. Lab-on-a-chip platforms present opportunities to reduce the need for manual handling of the analyses and experiments. Typical dimensions of microfluidic chips range from millimetres to a few centimetres. The small size of a lab-on-a-chip platform reduces the number of required reagents, solvents and biological samples, which also reduces the overall cost and time required for analysis. The efficiency of microfluidic-based methods can be much higher than that of conventional laboratory methods due to the possibility of controlling and manipulating fluids along with cells and other small particles within microsystem structures. Hence, they reduce the need for manual handling of the analyses and experiments and limit the requirements for highly trained staff [1–3]. However, lab-on-a-chip devices still need macroscale, often bulk, measurement setups with detection systems, imaging instruments such as microscopes and other large-scale functional components (e.g. fluid and gas

* Author to whom any correspondence should be addressed.

flow controllers, or micromanipulators). To realise truly portable and automatic microsystems that can be commercialised, there is a need to reduce the size of the instruments accompanying the microfluidic chips. Due to the popularity of optical detection methods and microscope-based imaging techniques in microfluidic systems, there is an especially high demand for integrating optical systems with lab-on-a-chip platforms [4, 5].

Standard bench-top optical microscopes, equipped with a camera and sets of bulky lenses, are widely used as imaging tools for lab-on-a-chip platforms. The size and weight of standard microscopes often limits the portability of the whole microsystem device. Due to the lack of standardisation of the geometry of lab-on-a-chip systems, as well as the casings in which they are put, it is necessary to individually adjust the microscope table settings and change parameters such as focus for each sample. There is also a need to immobilise the additional components such as fluid and gas tubes or electrical connection cables on the microscope table. This is a big disadvantage, especially if we are forced to move the microfluidic chip between the various measuring setups or change the analysed sample outside the microscope station [6–8].

Analysis of the existing state of knowledge shows that research on simplification of the imaging instrumentation and the methodology for image acquisition and post-processing is dynamically developed. However, there are several limitations to existing solutions. The imaging techniques for microsystems are still conducted only for transparent fluidic-based microsystems, usually made of glass or polymers [9–16]. Furthermore, microstructures reported in the literature are characterised by a simplistic architecture and are equipped in passive components such as microchannels. An additional challenge is microsystems that contain in their structure active and light-transparent components such as microbeams or diaphragms.

On the other hand, in recent years attempts have been made to replace classical imaging techniques based on microscopes or that require complex optical systems, where the construction and adjustment of all optical elements (mirrors or lenses) is complicated and requires a lot of space. Recently, there has been growing research interest in developing compact or on-chip optical imaging techniques that can overcome the limitations of standard microscopy described previously. Since all imaging techniques described here are developed to replace the classical method based on the use of a microscope, they are frequently described as microscopes-on-chip (MOC) techniques. Among existing MOC methods we can distinguish two main categories: transillumination and fluorescence microscopy. Each category can be further divided into various microscope techniques, such as bright-field, phase contrast, holographic and so forth [8].

The transillumination MOC category contains imaging techniques in which the light source is positioned on one side of the sample and the detector is on the opposite side. The light is transmitted through a chip and the specimen. To be able to use this method, the microsystem must be made of transparent material such as glass or polydimethylsiloxane. The light source used in this category may be coherent (lasers) or incoherent (light-emitting diodes, LEDs), depending on the technique used. In order to obtain partially coherent light, some researchers use a pinhole mask with a diameter of 50–300 μm and place the light source in front of it [3]. To minimise the noise signal coming from light scattering through the transparent microstructures, aperture covers made of hole arrays are placed on top of the microsystem platform directly above the imaging area [2].

Most methods do not use lenses to minimise the size of their setup and integrate the imaging system with the microfluidic platform as much as possible. The lack of optical magnification limits the spatial resolution by the pixel size of the image sensor. For this reason, the geometry of the imaging setup is crucial to obtain an imaging field of view equal to the active area of the image sensor chip. The general rule for an on-chip configuration is to put microsystem as close as possible to the image sensor (typically $\sim$100–1000 μm), and to place the light source at a sufficiently large distance from the test sample, usually of the order of a few centimetres [17]. Commonly used sensors are a complementary metal–oxide semiconductor (CMOS) chip or a charge-coupled device (CCD). The pixel size of CMOS or CCD cameras ranges from 2.2 to 20 μm.

Transillumination MOC combined with microfluidic circuits was successfully applied in various research works investigating biological specimens including cytometry, from blood cells to *Caenorhabditis elegans* [8]. To the best of the authors' knowledge there are no reports on the application of transillumination MOC to image-based porcine oocyte deformation measurements. Microscopic observation of porcine oocytes is a standard methodology for maturity assessment, classification, prediction of successful *in vitro* fertilisation and further embryo development [18, 19]. Only microscopic morphological observations enable non-invasive and real-time quality assessment. In recent work we developed a method to determine oocyte deformation on the basis of collected oocyte images during controlled squeezing [20]. Thus, image-based analysis of porcine oocytes is an important and widely used research tool.

In this paper, we present an integrated lab-on-a-chip transillumination MOC cytometer for observation of oocyte deformation. The system was obtained by fabrication of a silicon membrane with an integrated glass window for cell illumination and specialised software for holographic image processing and analysis. The results showed that significantly simpler optical instrumentation in comparison with a bulky microscope combined with hybrid silicon/glass membrane can be used for oocyte examination. Special attention in this paper was paid to the technology of the silicon/glass membrane as an innovative technology proposed here for the first time.

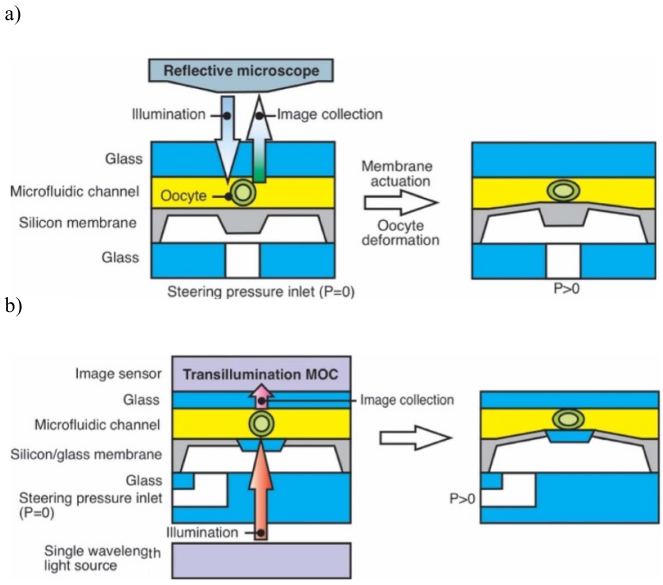

Figure 1. Lab-on-a-chip cytometers for porcine oocyte deformation characterisation. (a) The construction described in [18] with a silicon membrane and co-working with reflective microscope. (b) The construction described here using a transillumination MOC and silicon/glass membrane.

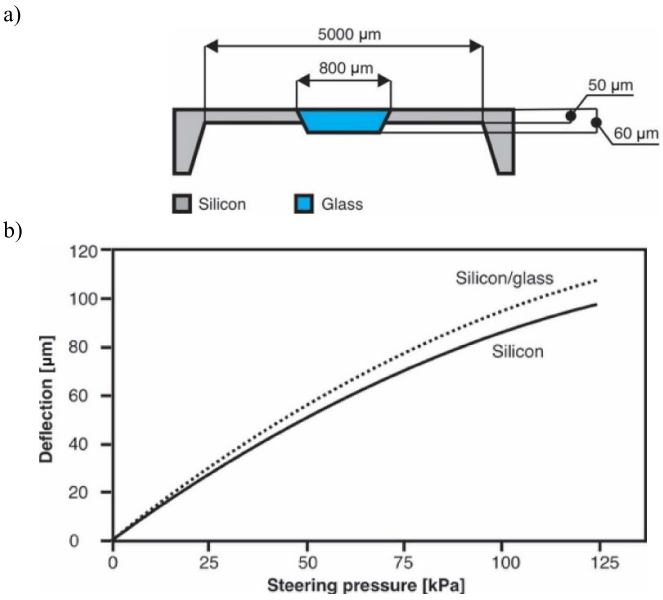

Figure 2. Silicon/glass membrane: (a) schematic drawing with the main dimensions, (b) membrane deflection as a function of actuation pressure for silicon and silicon/glass membranes—results of COMSOL simulation.

2. Transillumination lab-on-a-chip deformation cytometer

The lab-on-a-chip cytometer already developed by us [20] and the newly developed one described here are graphically compared in figure 1. The main differences are: (1) application of a simple optical circuit for oocyte illumination and image collection (transillumination microscope) that requires (2) fabrication of a silicon membrane for controlled oocyte deformation but with a glass window for cell illumination. Thus, the critical and unique component of the new cytometer is the silicon/glass membrane.

The overall design assumptions for the cytometer are the same as described by us for a micro-electro-mechanical system (MEMS) cytometer [20]. Briefly these include the diameter of the examined oocyte (from 90 to 130 μm) and the dimensions of the bossed membrane (50 μm thick, 5 mm $\times$ 5 mm area with a 0.8 mm $\times$ 0.8 mm boss forming a flat area for membrane deflection). With these dimensions the membrane should deflect by 100 μm when an actuating pressure of around 100 kPa is applied.

2.1. Silicon/glass membrane fabrication and cytometer assembly

The most important part of the cytometer is the silicon membrane with an embedded glass window. A schematic drawing of the silicon/glass membrane is shown in figure 2(a). The silicon membrane was first designed using AutoCAD and simulated with COMSOL Multiphysics. The deflection versus actuation pressure characteristic of the membrane was slightly smaller for a solid silicon bossed membrane than for membrane with a silicon/glass boss (figure 2(b)). This is because the glass (Schott, Borofloat 3.3) has a smaller Young's modulus than (100) silicon. However, the required membrane deflection range up to 100 μm was achieved. Once the simulation results confirmed proper operation of the silicon/glass membrane, the fabrication procedure started.

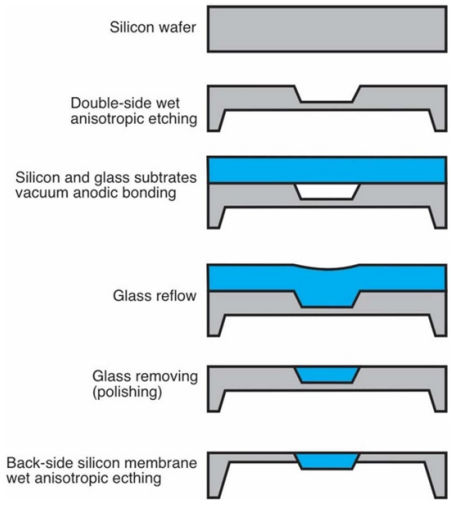

Figure 3. Main steps in producing the silicon/glass membrane technology.

A simplified step-by-step diagram of the membrane technology is shown in figure 3. It is based on two deep wet anisotropic etching processes of (100)-oriented, 380 μm thick, double-side polished monocrystalline silicon in 40% KOH at 80 °C. In the first double-side etching a 260 μm thick membrane was fabricated.

A cavity for the glass window was formed on the top side of the wafer. The main membrane was initiated by etching on the bottom side. Next, vacuum ($\sim 10^{-3}$ mbar) anodic bonding of a 0.5 mm thick borosilicate glass substrate (Borofloat 3.3, Schott, Germany; 450 °C, 2 kV) and a previously micromachined silicon substrate was carried out. In the next step, glass reflow (800 °C, 1 h) was carried out according to a previous procedure optimised by us for the fabrication of glass microlenses or prisms [21, 22]. Next, the redundant glass layer was removed (mechanically polished) from the top side of the thick membrane. Finally, the silicon membrane was thinned from the back side (etched in 40% KOH at 80 °C) to expose the glass window and to obtain a 50 μm thick membrane. As result of the described procedure, a deflectable silicon/glass membrane with a light-transparent window was achieved. The aperture of the glass window was about 0.72 mm × 0.72 mm.

The other components of the cytometer (0.5 mm and 2 mm thick glass substrates) were processed according to procedure described in [20] to fabricate the microfluidic part of the cytometer and actuation microchamber. Briefly, two additional glass substrates were micromachined to form the structure of the cytometer. A microfluidic channel for the introduction and extraction of oocytes to/from a measurement chamber as well as a trap for precise oocyte positioning in relation to the silicon bossed membrane were micromachined in a single process by wet etching of the first glass substrate. A pressure steering chamber and pressure inlet for actuation of the silicon membrane were drilled or etched in the second glass substrate. Finally, two glass substrates and the silicon part with the membrane were anodically bonded to each other to form the multilayer silicon/glass lab-on-a-chip cytometer. The cytometer was mounted in a 3D printed housing, enabling cooperation with the optical system and pressure actuation unit (Elveflow, OB1 Mk3 pressure controller).

2.2. Optical setup and data processing/analysis software

The optical system contains a LED module (430 nm, 490 mW, Thorlabs, Sweden) coupled with 125 μm glass fibre (Thorlabs, Sweden) and combined with a 50 μm aperture at the fibre outlet working as a single-wavelength illumination light source. The aperture was placed 5 cm from the top side of the cytometer. The cytometer was placed directly on the surface of a 5.5 mm × 3.3 mm CMOS sensor as the image collector (Sony Exmor CMOS Sensor). The pixel resolution of the CMOS sensor was 1920 × 1080 pixels. Thus, a single pixel has a dimension of around 2.5 μm. The image sensor was connected by USB to a personal computer. The CMOS sensor was placed directly on the surface of the chip. The distance between the image sensor and oocyte trap was 0.5 mm. A schematic of the optical system is shown in figure 4.

The second important component of the detection system is the software developed for image analysis. In our previous works on cell image analysis and porcine oocyte deformability the software enabled determination of various parameters—oocyte outer/inner diameter, entire oocyte and ooplasm area and thickness of the zona pellucida [20]. This was achieved by various edge detection algorithms. In the case of holographic images, three algorithms for edge detection were considered: simple edge detection, multiple thresholding and an alpha-form algorithm [23].

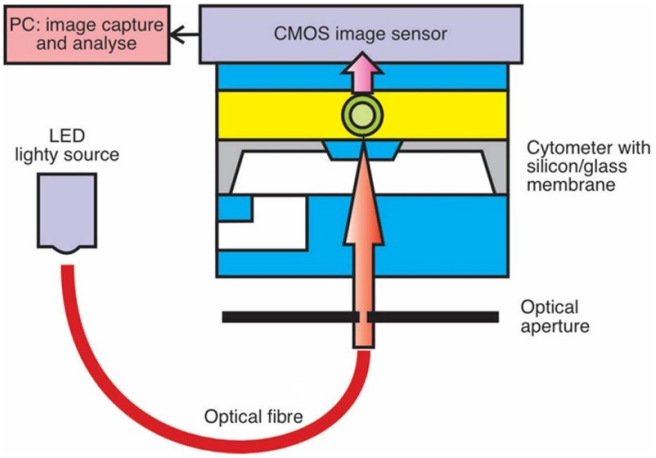

Figure 4. Scheme of the optical set up.

The software was implemented using the C++ language with the OpenCV3 programming library for efficient image processing. The grey-scale intensity cross-section of the image containing a holographic representation of oocyte was produced as another simple image analysis method. In our previous work we concluded that the most representative parameters for determining the deformability were outer/inner diameters and zona pellucida thickness [20].

2.3. Porcine oocyte processing

In preliminary experiments, agarose beads (Agarose Bead Technologies, USA) with diameters from 50 μm to 150 μm were applied as models of the oocytes. In the main experiments porcine oocytes were examined. Post-mortem ovaries from 5- to 6-month-old gilts were collected at the slaughter house (Sokolow SA, Poland). The oocytes were processes as described in [20]. Only first-class oocytes were used in the experiments described here. A total of 20 oocytes were examined. Results of deformation experiments for membrane actuation pressures up to 100 kPa were compared with those for the earlier on-chip MEMS cytometer developed by us.

3. Results and discussion

A silicon membrane with an embedded glass window was successfully fabricated (figure 5). Images of the glass window from both membrane sites showed proper filling of the silicon cavity with glass (figure 5(b)). The glass window was transparent to light without a milk-like internal structure. The view of the glass structure when almost all the silicon membrane was etched away showed perfectly reflected geometry of the silicon cavity with (111) and (100) walls (figure 5(c)). The membrane

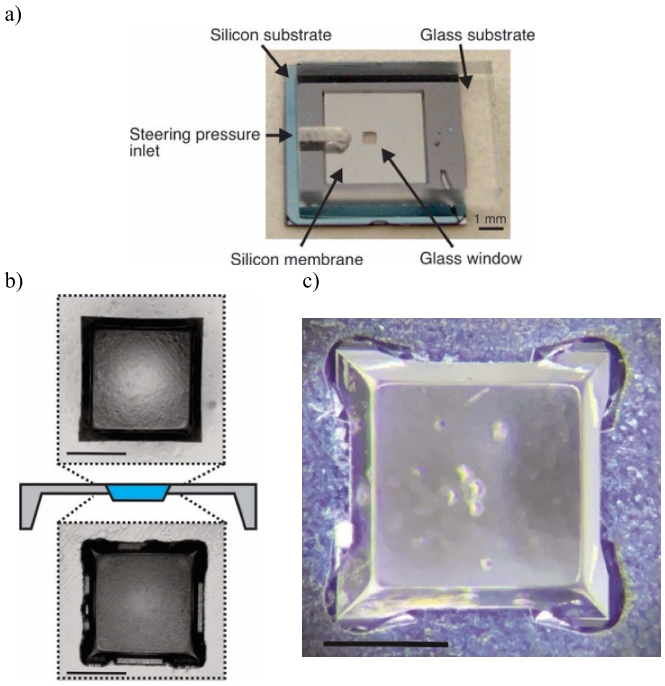

Figure 5. Silicon/glass membrane. (a) View of the membrane with a glass window and bonded to a bottom glass substrate with a steering pressure inlet. (b) Top and bottom views of the glass window. (c) The glass window in the membrane (membrane thickness around 5 μm, just before the membrane was etched away) with characteristic (100) and (111) silicon plane mould. Scale bar 200 μm.

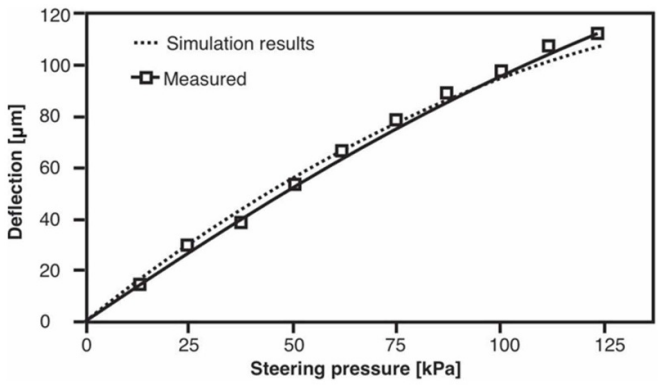

Figure 6. Real and simulated silicon/glass membrane deflection as function of steering pressure.

was bonded to the glass substrate with a steering pressure inlet (figure 5(a)).

Real deflection of the membrane versus actuating pressure was measured using a fibre optic distance sensor (Philtec Inc., USA) (figure 6). Measured characteristics were similar to the results of COMSOL simulations. The tightness of the silicon/glass interface of the window was checked by immersion of the bonded structure in water during pressure actuation (100 times actuation; up to 200 kPa). No generation of air bubbles from the silicon/glass interface was observed.

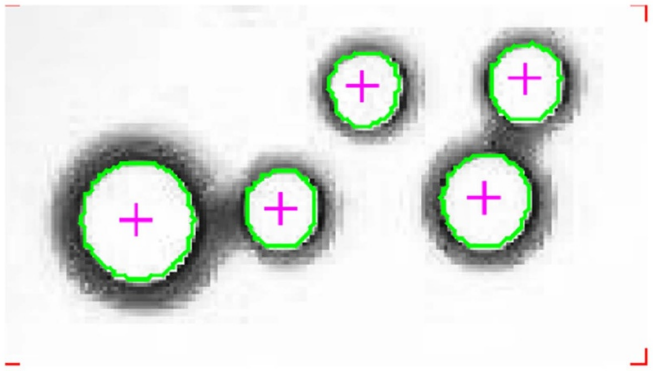

Figure 7. Image of the agarose beads (diameters from 50 μm to 150 μm) after image analysis with an edge detection algorithm (centres of the beads and outside contours are marked).

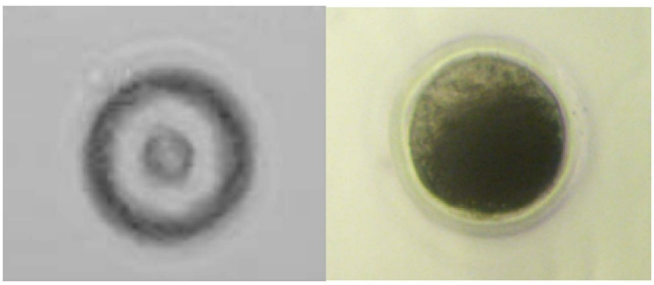

Figure 8. Porcine oocyte images as captured by the cytometer presented here with a silicon/glass membrane (left image) and the MEMS cytometer described in [18] (right image). Oocyte diameters are about 120 μm.

The first image collection experiment was carried out with agarose beads. The internal part of the bead image was uniform and bright, whereas the outer halo was dark with a thickness dependent on the bead diameter. It was possible to distinguish single beads and two or more beads close to each other (figure 7) using the applied analysis algorithms.

Examples of captured images of a single non-deformed oocyte obtained by the cytometer presentedhere compared with an image obtained by a MEMS cytometer co-working with an inverted biological microscope are shown in figure 8. Images of the oocyte illuminated through the silicon/glass membrane are hologram-like with distinguishable circles formed by the internal structure of the oocyte interacting with light. The holographic image is the result of the lens-free optical configuration and the image was created by the interference of waves scattered by the object with the background light, which acts as the reference wave [24]. The non-uniform optical structure of the oocyte compared with uniform agarose beads also had a part in creation of the image. The outer diameter of the oocytes was very difficult to observe without software analysis of the image.

Oocyte images were analysed by the three algorithms mentioned earlier and the cross-sectional intensity graph (figure 9).

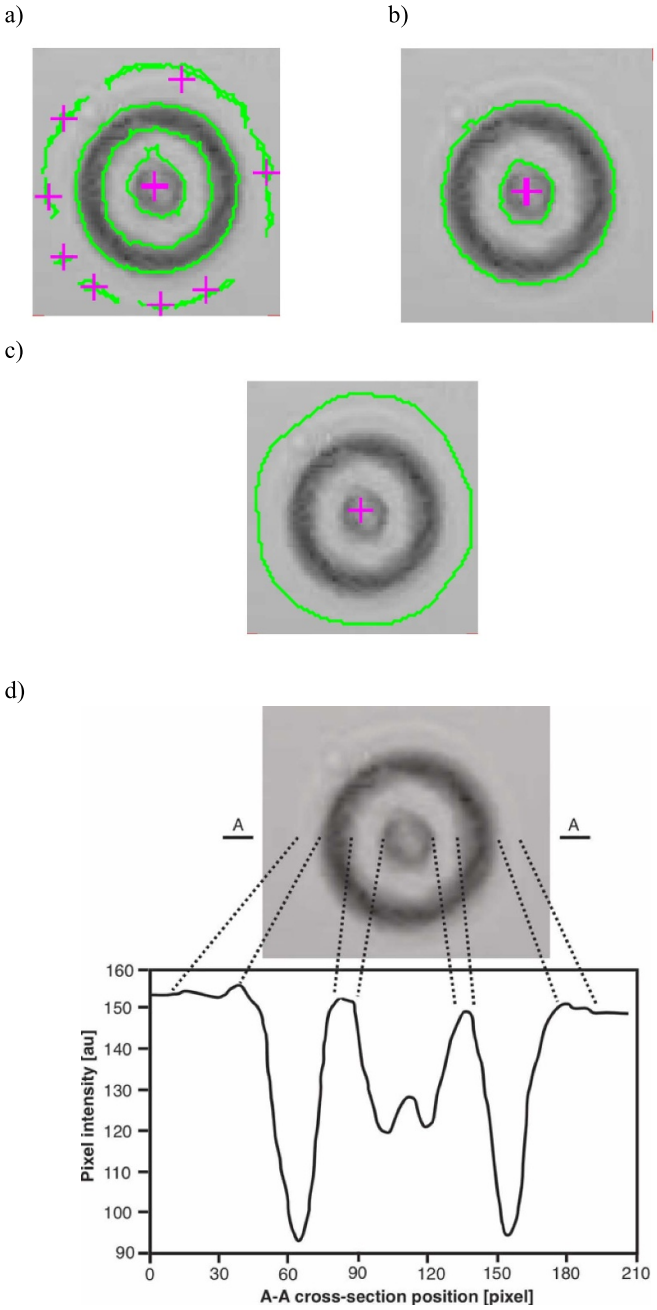

Figure 9. Results of oocyte image analysis by (a) a simple edge detection algorithm, (b) the multiple thresholding algorithm, (c) the alpha-form algorithm and (d) A–A cross-section pixel intensity with a view of the examined oocyte and distinguishable intensity regions.

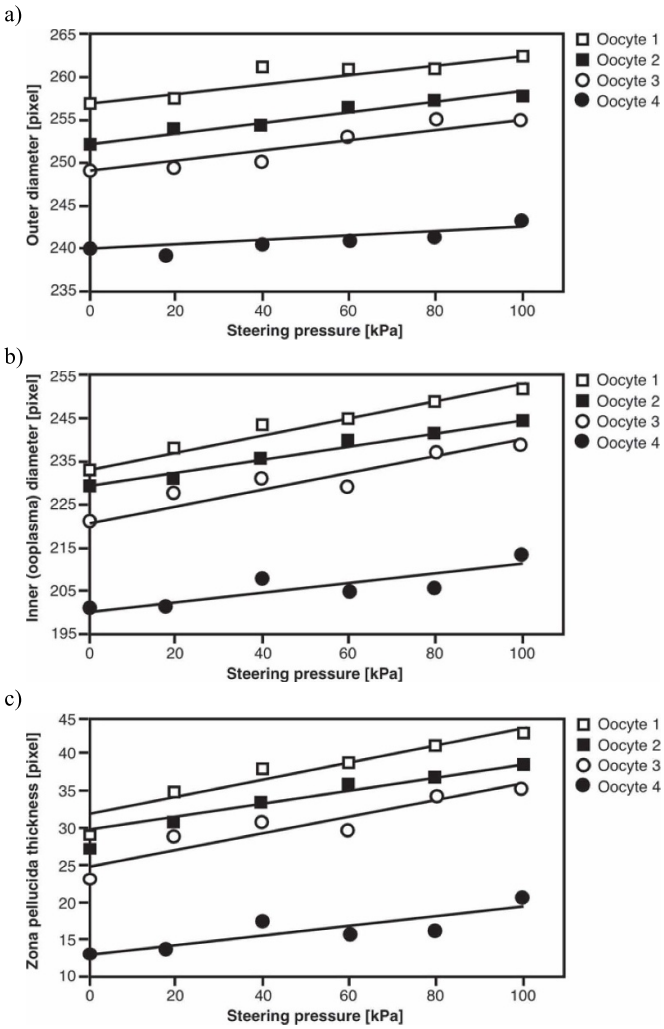

Figure 10. Results of porcine oocyte deformation experiments determined on the base of image analysis of oocyte parameters versus membrane actuation pressure (results for four example oocytes): (a) outer diameter, (b) inner diameter, (c) zona pellucida thickness.

The simple edge detection algorithm was not able to detect the proper outer sheath (figure 9(a)) but the inner parts were recognised. The multiple thresholding algorithm did not detect the outer sheath at all, but the inner elements were detected (figure 9(b)). The third algorithm, the alpha-form, properly recognised only the outer sheath (figure 9(c)). When the proper edge was detected, it was automatically estimated using a circle (Hough transform) of known diameter. The cross-sectional intensity of the oocyte was successfully obtained from clearly distinguishable regions of change of the light intensity (figure 9(d)). With this cross-section it was possible to determine outer/inner diameters of the oocyte. On the base of outer/inner diameter values the thickness of the zona pellucida can be calculated. Comparison of the values determined for the diameters by the applied algorithms and cross-sectional intensity showed them to be very similar (difference less than 5%) but the cross-section method seems to be the easiest, and enabled determination of all the required oocyte parameters.

Dependences of the outer diameter and ooplasm diameter (determined by alpha-form and multiple thresholding algorithms, respectively) and zona pellucida thickness as a function of membrane actuating pressure (membrane deflection) are shown on figure 10 for four example oocytes. Linear dependence was noticed (the same as for our previous MEMS cytometer experiments). The change in outer oocyte diameter

was from 1.6% to 2.8%, the inside diameter changed from 2.8% to 7.6% and the zona pellucida from 26% to 50%. The change in these parameters observed with the previous MEMS cytometer was 3%–4% for outside diameters, 5%–6% for inside ones and 45% for the zona pellucida [20]. Thus, similar results were obtained for both cytometer constructions.

4. Conclusions

In this paper we present for the first time the technology of a glass window integrated with a pressure-actuated silicon membrane. Proper micromechanical operation of the membrane and its light transparency (due to the embedded glass window) enabled development of a deformation cytometer for investigation of the mechanical properties of porcine oocytes. Images of the oocytes were collected by image sensors placed directly on the surface of the cytometer. The optical system worked in transillumination configuration and the captured images were holograms of the examined oocytes. Specialised image analysis software was developed, tested and successfully implemented. Due to the low resolution of the images and their holographic nature, specialised image analysis algorithms were applied. In future work it would seem that image processing supported by artificial intelligence should be applied. As a result of our work, a cytometer with transillumination configuration was successfully used to investigate porcine oocytes. The deformation results were in good agreement with our previous MEMS cytometer working with a reflective microscope. Changes in outer and inner oocyte diameters and zona pellucida thickness were comparable to the values determined by the MEMS cytometer. The simple lens-free configuration of the optical system makes it more compact and reliable than traditional bulky systems. Thus, a truly portable and point-of-care instrument for examination of oocyte deformation can be built in the future.

Data availability statement

All data that support the findings of this study are included within the article (and any supplementary files).

Acknowledgments

Work on the cytometer with a silicon/glass membrane were carried out under a project funded by the National Centre for Science PRELUDIUM (Project No. 2019/33/N/ST7/02459).

ORCID iDs

Aleksandra Pokrzywnicka https://orcid.org/0000-0002-9903-6390
Rafał Walczak https://orcid.org/0000-0002-9371-9414

References

[1] Chiu D, de Mello A, Di Carlo D, Doyle P, Hansesn C, Maceiczyk R and Wootton R 2017 *Chem* **2** 2201–23
[2] Samiei E, Tabrizian M and Hoorfar M 2016 *Lab Chip* **16** 2376–96
[3] Du G, Fang Q and Den Toonder J 2016 *Anal. Chim. Acta* **903** 36–50
[4] Kuswandi B, Huskens J and Verboom W 2007 *Anal. Chim. Acta* **601** 141–55
[5] Wu J, Zheng G and Lee L 2012 *Lab Chip* **12** 3566–75
[6] Zhu H, Osikman S, Mudanyali O, Greenbaum A and Ozcan A 2013 *Lab Chip* **13** 51
[7] Merola F, Memmolo P, Miccio L, Bianco V, Paturzo M and Fierro P 2015 *Proc. IEEE* **103** 2
[8] Paiè P, Vazquez R, Osellame R, Bragheri F and Bassi A 2018 *Cytometry* A **93A** 987–96
[9] Balsam J, Ossandon M, Kostov Y, Brick H and Rasooly A 2011 *Lab Chip* **11** 941–9
[10] Seo S, Isikman S, Sencan I, Mudanyali S, Su T, Bishara W, Erlinger A and Ozcan A 2010 *Anal. Chem.* **82** 4621–7
[11] Lee J, Kwak Y, Peak S-H, Han S and Seo S 2014 *Sens. Actuators* B **196** 511–7
[12] Roy M, Jin G, Seo D, Nam M-H and Seo S 2014 *Sens. Actuators* B **201** 321–8
[13] Paturzo M, Finizio A, Memmolo P, Puglisi R, Balduzzi D, Galli A and Ferraro P 2012 *Lab Chip* **12** 3073–6
[14] Mandracchia B, Bianco V, Wang Z, Mugnano M, Bramanti A, Paturzo M and Ferraro P 2017 *Lab Chip* **17** 2831
[15] Bianco V, Mandracchia B, Marchesano V, Pagiarulo V, Olivieri F, Copolla S, Paturzo M and Ferraro P 2017 *Light Sci. Appl.* **6** e17055
[16] Sobieranski A, Inci F, Tekin H, Yuksekkaya M, Comunello E, Cobra D, von Wangenhaim A and Demiric U 2015 *Light Sci. Appl.* **4** e346
[17] Zhang Y, Greenbaum A, Luo W and Ozcan A 2015 *Virchows Arch.* **467** 3–7
[18] Ubaldi F and Rienzia L 2008 *Placenta* **29** 115–20
[19] Sadani Z, Wcogne B, Pieralli C, Roux C and Ghatbi T 2005 *Sens. Actuators A* **121** 364–72
[20] Pokrzywnicka A, Śniadek P, Małyszka N, Lizanets D, Kubicki W and Walczak R 2019 *J. Micromech. Microeng.* **29** 095004
[21] Bargiel S, Walczak R, Albero J S, Dziuban J, Alkowska K, Nieradko Ł, Józwik M and Gorecki C 2006 *Proc. XX Eurosensors* pp 17–20
[22] Pokrzywnicka A, Śniadek P and Walczak R 2021 *J. Micromech. Microeng.* **31** 125009
[23] Lizanets D and Walczak R 2018 *Opt. Appl.* **48** 15–24
[24] Bishara W, Zhu H and Ozcan A 2010 *Opt. Express* **18** 27499